A Hybrid RFOA-DDAO Based Voltage Transfer Gain Enhancement through Ultra Lift Luo Converter and Cockcroft-Walton Multiplier

G. Merlin Suba[1*], Dr. M. Kumerasen[2]

Abstract: This manuscript proposes a novel hybrid strategy to enhance the voltage gain through an ultra-lift luo converter and Cockcroft Walton multiplier for driving electric vehicles smoothly. The proposed hybrid strategy is the joint execution of Red Fox Optimization Algorithm (RFOA) and Dynamic Differential Annealed Optimization (DDAO) and hence it is named as RFOA-DDAO system that creates the greater voltage transfer gain. Entire world is focusing on electric vehicle to reduce CO2 level in the environment. All renewable energy sources are of low voltage, but it is not enough to drive electric vehicle. So, interfacing equipment is needed as converter to enlarge the voltage gain from low voltage to high voltage to drive electric vehicle. Here, an output voltage variation as well as voltage deviation can be minimized using this proposed technique. Finally, the proposed approach is executed on MATLAB/Simulink working platform and execution result is compared with the existing techniques, like BOA and GPC methods.

Keywords: High voltage gain, Electric vehicle, Ultra lift luo converter, Cockcroft-Walton multiplier, Red Fox Optimization algorithm, Dynamic Differential Annealed Optimizations

1. Introduction

In recent days, the usage of fossil fuel is decreased due to their higher pollution issues. But electric vehicles (EVs) powered by battery systems are mostly utilized due to their minimum or zero polluting emissions [1]. However, the developed advancement of batteries able to give maximum performance for electric vehicles, the continuous charging or discharging current from batteries affects the reliability of battery and decreasing effectiveness [2]. The correlations of battery with super-capacitor from hybrid energy storage system of electric vehicles are assumed better solution for enhancing total vehicle efficiency with battery life. Super-capacitor has benefits of higher power density [3], higher life cycle, better charge or discharge efficiency. It also gives a maximum transmission power virtually as faster and suitable for immediate EV power variations [4-7]. Supercapacitors deliver power for acceleration and regenerative braking on battery power, meeting the need for maximum energy storage density of wide-range operation. Therefore, a bidirectional dc-dc converter using broad voltage gain is selected for hybrid energy storage system (HESS) to interconnect less voltage super capacitors using maximum voltage DC bus [8-10].

Generally, a high voltage gain is needed to drive that electric vehicle as smoothly [11-13]. It is only possible through the utilization of effective converters. The various types of converters are developed and utilized in the electric vehicle applications like luo type converters, boost converters, bidirectional converters, etc [14]. The voltage Lift (VL) method is utilized in luo converters to provide an output voltage maximizing either in arithmetic or geometric process at every stage. VL method is basically accepted in switching circuit as well as supplies maximum output voltage with improved circuit features [15-17]. In luo converters, a capacitor is powered and located on top for producing maximum output voltage. The self-lift, re-lift, triple-lift along with quadruple-lift converters could be implemented from elementary topology. An ultra-lift luo converter gives maximum output voltage gain compared with other luo converters [18-22].

In addition, because of the requirement of high voltage in higher energy physics along some types of protective research, voltage multipliers are mostly utilized in many applications. In previous decades, transformers are mostly utilized to boost the voltage [23-26]. The output from the secondary coil of the transformers improves the voltage but which reduces the current and generates higher deviations. Then different hardware circuits were implemented which gives higher voltage conversion ratio, less output voltage ripple, high efficiency, simple structure and minimum cost. Among these, the cockroft-walton multiplier is mostly utilized which has the capability of generating higher DC voltage as minimum voltage AC or DC input [27-29]. The cockroft-walton multiplier has number of stages and each stage of the circuit contains capacitors and diodes. Rest of this manuscript is structured as: section 2 describes the recent research works, section 3illustrates the voltage gain improvement configuration using proposed converter and multiplier, section 4 portrays the proposed model of RFOA-DDAO, section 5 demonstrates the result and discussions, section 6 presents the conclusion.

2. Recent research work: a brief review

Several works were already presented in the literature depending on high voltage gain converters for driving the electric vehicles.

---
[1] *Research Scholar, Department of Electrical and Electronics Engineering, Dr. M.G.R Educational and Research Institute, Chennai, Tamil nadu, India, ORCID ID: 0000-0002-8048-9808*
[2] *Professor, Department of Electronics and communication Engineering, Dr.M.G.R Educational and Research Institute, chennai, Tamil nadu, India, ORCID ID: 0000-0002-2527-357X*
* Corresponding Author Email: gmerlinsuba0610@gmail.com

Some of them are:

Lee et al., [30] have presented an isolated bi-directional PWM resonant converter for V2G (H) EV on-board charger. The PWM-RCs have super switching features, but which not suitable for bi-directional applications due to that works under buck-type operation in spite of power transmission directions. This problem may be rectified through structure change techniques that double the gain of the converter. Furthermore, the extra methods to improve the converter gain during the discharge process were demonstrated by analyzing the gain characteristics. The efficiency of the bidirectional PWM-RC was analyzed using 6.6 kW prototype charger. Zhang et al., [31] have demonstrated the DC-DC boost converter including broad input range and maximum voltage gain for fuel cell vehicles. To relate the fuel cell output voltage to dc bus voltage, a new dc-dc boost converter by a long input range with maximum voltage gain was introduced to function as needed power interface that lowers voltage stress. A prototype with a nominal power of 300W / 400V was implemented and the highest proficiency of the introduced converter was computed as 95.01% at 300W. Zhang et al., [32] have demonstrated the broad input voltage range quasi-z source boost dc-dc converter using maximum voltage gain for fuel cell vehicles. The presented converter has the ability to achieve maximum voltage gain using broad input voltage range, then providing a minimum voltage stress across all equipment. The performance of an introduced converter was related with other converters. A scaled-down 400V/400W prototype was implemented for validating the introduced method.

Zhang et al., [33] have presented a DC-DC converter using broad range of voltage gain for hybrid power sources. A quasi-z source switched capacitor switched hybrid bi-directional DC-DC converter was introduced for electric vehicles having high voltage gain in bi-directional power transmissions. Related to the basic quasi-z source bidirectional dc-dc converter, the introduced converter only modulates the location of major power switch and connects the switched capacitor cell on the output side. Therefore, the benefit of the high voltage gain was achieved, also the minimum voltage stress across the power switches. Leyva-Ramos et al., [34] have demonstrated a control approach of quadratic boost converter using voltage multiplier cell for maximum voltage gain. A quadratic boost converter was coupled through voltage multiplier cell and an output filter provided the maximum voltage gain. The equation of the capacitor voltages and the currents of the inductors with equivalent variations that allow the optimal design of the converter were expressed. A step-by-step procedure was provided for setting a controller in current mode. Lai et al., [35] have suggested the development of bi-directional DC / DC converter with double battery energy storage for the hybrid EV system. An input converter has ability to work in both upstream and downstream mode. In addition, the model could independently control the power transmission among two minimum voltage sources. The circuit configuration, operation, steady-state analysis, and closed-loop control of the introduced bidirectional DC-DC converter were demonstrated depends on three power transmission modes. Zhang et al., [36] have demonstrated an ordinary ground quasi-z switched source bidirectional DC-DC converter using broad voltage gain range for electric vehicles. An introduced converter was based on a two-level basic quasi-z source bidirectional DC-DC converter that varies location of main power switch. That has the benefits of a high voltage gain, a minimum voltage stress across the power switches.

2.1. Background of the Research Work

The review of the current investigation operation portrays that, a high voltage gain converter for drive the electric vehicle as smoothly is an important contributing factor. The different types of converters are implemented for enhancing voltage gain for properly running the electric vehicles, like isolated bidirectional PWM resonant converter, DC-DC boost converter, quasi-z source boost DC-DC converter, Hybrid switched-capacitor/switched-quasi z-source bidirectional DC–DC converter, quadratic boost converter, etc. The PWM-RCs has best switching characterizes and improve the voltage gain. But it works under buck type operation in spite of power transmission directions, thus it not suitable for bidirectional applications. The DC-DC converters are utilized to tune that voltage and small count of equipment's is required for making this converter. But this converter generates the noise and the costs of equipment's are high. A quasi-z source boost DC-DC converter has high continuous input current along with less voltage stress, but it has higher output voltage variations. Therefore an ultra-lift luo converter and cockroft-walton multiplier is implemented to overcome these problems. Also a hybrid RFOA-DDAO technique is implemented with an ultra-lift luo converter and cockcroft-walton multiplier to achieve the objective functions in optimal manner. Several works were presented in the literature to solve these issues, but the presented works are not much effective; these disadvantages and issues have prompted to do this research work.

3. Configuration of voltage gain improvement using proposed converter and multiplier

Figure 1 portrays that implementation diagram of proposed system. The implementation diagram consists of ultra-lift luo converter, cockroft-walton multiplier and electric vehicle. The electric vehicle contains different types of components like electrical motor, audio devices, lights [37] etc. The certain amount of voltage is need for running these devices. The DC output voltage provided by the conventional converter has maximum voltage ripple and it is not stable. Due to high voltage variation, the devices of EV are being affected. So, the proper voltage gain is most important for running the electric vehicle with smoothly. In this regard, the maximum voltage gain DC-DC converter is implemented on research work. The multiple number of maximum voltage gain DC-DC converters are available for EV uses. But in this research work, an ultra-lift luo converter is selected from proposed converter due to its number of advantages. The ultra-lift Luo converter has simple structure with a single switch to give higher output. The switching loss is minimum compared with other converters and this type of converter is more appropriate for electric vehicle and battery-operated vehicle. The main aim of this work is to improve that voltage gain of EV through the minimization of error by the help of proposed technique with an ultra-lift luo converter and diode-capacitor cockroft-walton multiplier. In addition, a hybrid algorithm is implemented to optimally enhance the DC voltage gain for smooth running of electric vehicles (EVs). The proposed hybrid algorithm is the joint execution of both the Red Fox Optimization algorithm (RFOA) and Dynamic Differential Annealed optimization (DDAO) Algorithm. The mathematical modelling of components used in the proposed system is explained under below section.
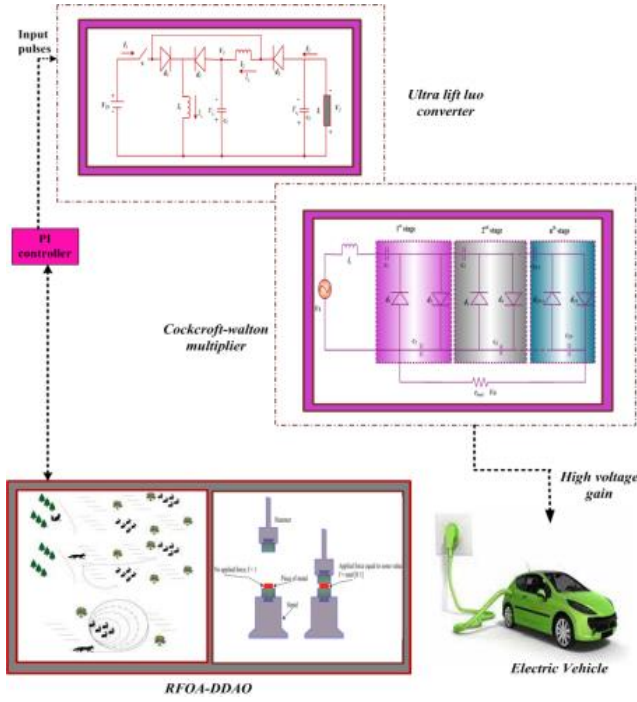
Figure 1. Implementation diagram of proposed system

In this research work PI (Proportional Integral) controller is implemented to create pulses for switch. For controlling converter output voltage, the converter output voltage with multiplier is detected then error voltage is created subsequent to the comparison of detected voltage with stable reference voltage. This error signal is processed with PI controller that creates output control signals like proportional gain (k_p) and integral gain (ki). The generated control signals are given to the proposed RFOA-DDAO technique. Then the best control signal value is taken from the proposed technique and after that which is provided with ultra-lift luo converter through PI controller, to optimally enhance that voltage transfer gain.

3.1. Modelling of Renewable Energy Sources (RES) and Components of Smart Grid (SG) System

The electric vehicle (EV) model is incorporated with the driver design, power train design and vehicle dynamics design. In the driver model the input is taken as real speed which is distinct with the reference speed. In the power train design accept the input from the driver model. Based on the location of the brake pedal with accelerator pedal the outcome of driver model is obtained. The driver pedal position is achieved by the power train which is used to manage the energy of the system. Based on the force of vehicle, dynamic model processes the vehicle with real speed. The vehicle forces such as traction force, aerodynamic drag force, rolling resistance force, and force of gravity. The following equation describes the charging with discharging power limits of EV [38].

$$cr^{ev,MIN} \times \tau^{ev}_{I,T,\varpi} \le P^{ev,CH}_{T,\varpi} \le cr^{ev,MAX} \alpha^{ev}_{I,T,\varpi};$$
$$\vee I \notin i, T \notin \left[t_I^{ARR}, t_I^{DEP} \right], \varpi \notin \Psi \quad (1)$$

$$dr^{ev,MIN} \times \left(1 - \tau^{ev}_{I,T,\varpi}\right) \le P^{ev,CH}_{T,\varpi} \le dr^{ev,MAX}\left(1 - \alpha^{ev}_{I,T,\varpi}\right);$$
$$\vee I \notin i, T \notin \left[t_I^{ARR}, t_I^{DEP} \right], \varpi \notin \Psi \quad (2)$$

The state-of-energy of EV at time T and starting stage can be expressed as,

$$SOE^{ev}_{I,T,\varpi} = SOE^{ev}_{I,T-1,\varpi} \times \eta^{ev,CH} \times \frac{P^{ev,CH}_{I,T,\varpi}}{\nabla t} - \frac{P^{ev,DISCH}_{I,T,\varpi}}{\nabla t}; (3)$$
$$\vee I \notin i, T \notin \left[t_I^{ARR}, t_I^{DEP} \right] \varpi \notin \Psi$$

$$SOE^{ev}_{I,T,\varpi} = SOE^{ev,ARR}_I \times \eta^{ev,CH} \times \frac{P^{ev,CH}_{I,T,\varpi}}{\nabla t} - \frac{P^{ev,DISCH}_{I,T,\varpi}}{\nabla t}; (4)$$
$$\vee I \notin i, T = t_I^{ARR}, \varpi \notin \Psi$$

$$SOE^{ev}_{I,T,\varpi} = SOE^{ev,MAX}_I; \vee I \notin i, T \notin \left[t_I^{ARR}, t_I^{DEP} \right], \varpi \notin \Psi \ (5)$$

$$SOE^{ev}_{I,T,\varpi} = SOE^{ev,MIN}_I; \vee I \notin i, T \notin \left[t_I^{ARR}, t_I^{DEP} \right] \varpi \notin \Psi \ (6)$$

The minimal state-of-energy for EV upon their departure time can be expressed as,

$$SOE^{ev}_{I,T,\varpi} = SOE^{ev,DEP}_I; \vee I \notin i, T = t_I^{DEP}, \varpi \notin \Psi \ (7)$$

where, $cr^{ev,MIN}$ is the minimum EV charging rate, $dr^{ev,MIN}$ refers minimal EV discharging rate, $\eta^{ev,CH}$ is discharging EV efficiency, $P^{ev,CH}_{I,T,\varpi}$ refers charging power of Ith EV, $P^{ev,DISCH}_{I,T,\varpi}$ refers discharging power of Ith EV, Ψ represent the number of scenarios, i represent count of EVs, t represent count of time slots, ϖ is index values (ϖ =1, 2, 3,… Ψ), $SOE^{ev,MIN}$ and $SOE^{ev,MAX}$ is the minimal state of energy of EV, $SOE^{ev,ARR}_I$ and $SOE^{ev,DEP}_I$ is the state of energy of Ith EV at arriving and state of energy of Ith EV at departing.

3.2. Modelling of Ultra Lift Luo Converter

An ultra-lift (UL) method gives high voltage transfer gain to other converters. Also, an ultra-lift luo converter has an ability to minimize the voltage ripples and has more efficiency. The state-space model is general technique for describing the physical system. It helps to understand the varying characteristics of a system. The state-space modelling of an ultra-lift luo converter is explained on this section.
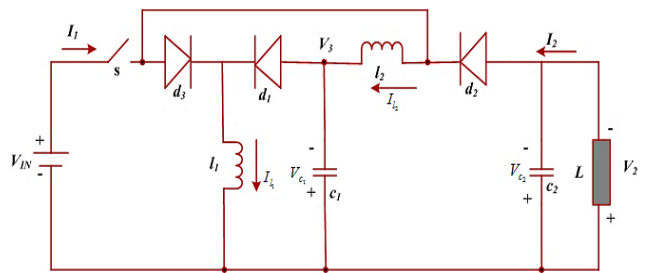

Figure 2. Equivalent circuit of ultra-liftluo converter [39]

The ultra-lift luo converter gains maximum output transfer gain by geometric process. Fig 2 portrays that equivalent circuit of ultra-lift luo converter. It contains a single switch (s), two inductors namely l_1 ,l_2, two capacitors c_1 , c_2, three diodes d_1, d_2, d_3 and load r. The ultra-lift luo converter input voltage and currentisV_{IN}andI_1, the output voltage and current is V_2 and I_2, the conduction duty cycle D and the switching frequency f. As a result, there petition period $t=1/f$, switch on period Dt along with the switch off period is $(1-D)t$. If the switch is on condition, input inductor current starts to increase through slope of $+V_1 / l_1$ at continuous conduction mode, it is reduced with the slope of $-V_3 / l_1$ when the switch is turned OFF. Also, it gives high gain compared with other

converters and the power deviation is reduced while the power transmission. Here, input power is similar with output power or $V_1 \times I_1 = V_2 \times I_2$.

$$Dt\left(\frac{V_1}{l_1}\right) = (1-D)t\left(\frac{V_3}{l_1}\right) \tag{8}$$

Thus, voltage across capacitor c_1 is,

$$V_{c_1} = V_3 = \frac{D}{(1-D)} * V_1 \tag{9}$$

The current through inductor l_2 is maximizes using slope $+(V_1 - V_3)/l_2$ during switch ON and diminishes using slope $-(V_3 - V_2)/l_2$ through switch OFF. At steady state, the increase in current is similar with decrease in an entire period t.

$$Dt\left(\frac{V_1 + V_3}{l_2}\right) = (1-D)t\left(\frac{V_2 - V_3}{l_2}\right) \tag{10}$$

The output voltage of converter may be expressed,

$$V_2 = \frac{D}{(1-D)} * \frac{(2-D)}{1-D} V_1 \tag{11}$$

The voltage transfer gain of ultra liftluo converter is expressed as,

$$Gain = \frac{V_2}{V_1} = \frac{D}{(1-D)} * \frac{(2-D)}{1-D} = \frac{D(2-D)}{(1-D)^2} \tag{12}$$

The voltage transfer gain of ultra-lift luo converter is greater to other converters. The ultra-lift luo converter modes of operation are explained below.

3.2.1. ON-Mode

The ultra-lift luo converter circuit diagram in ON-mode demonstrates at figure 3. In this mode, the Switch (s) is turned ON. Also, diode d_2, d_3 obtains reverse biased and energy saved in inductor and capacitor.
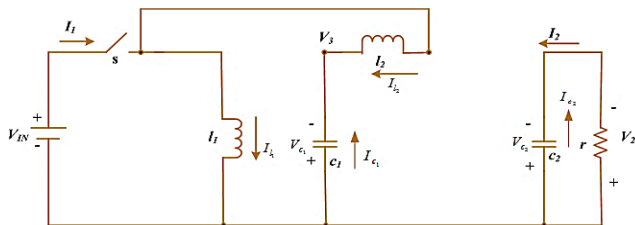

Figure 3. Equivalent circuit of ultra-lift luo converter at ON-mode [39]

The state equations of this mode can be articulated [39],

$$l_1 \frac{\partial I_{l_1}}{\partial T} - V_{IN} = 0 \tag{13}$$

$$l_2 \frac{\partial I_{l_2}}{\partial T} - V_{c_1} - V_{IN} = 0 \tag{14}$$

$$c_1 \frac{\partial V_{c_1}}{\partial T} + I_{l_2} = 0 \tag{15}$$

$$c_2 \frac{\partial V_{c_2}}{\partial T} + \frac{1}{r_0} V_{c_2} = 0 \tag{16}$$

State space matrix model of ultra-lift luo converter in ON condition as follows,

$$\begin{bmatrix} I_{l_1} \\ I_{l_2} \\ V_{c_1} \\ V_{c_2} \end{bmatrix} = \begin{bmatrix} 0 & 0 & 0 & 0 \\ 0 & 0 & \frac{-1}{l_2} & 0 \\ 0 & \frac{-1}{c_1} & 0 & 0 \\ 0 & 0 & 0 & \frac{-1}{c_{2r_0}} \end{bmatrix} \tag{17}$$

3.2.2. OFF-Mode

The ultra-lift luo converter circuit diagram in Off-mode portrays at figure 4. The Switch (s) are turned OFF along with diode obtains forward biased. It sends their stored energy into capacitor c_2 with help of diode. Similarly, inductor l_1 sends that stores power into capacitor c_2.
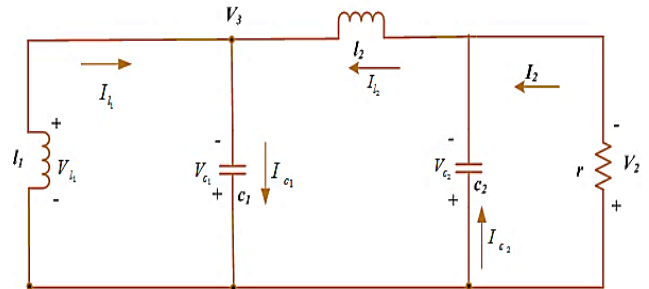

Figure 4. Equivalent circuit of ultra-lift luo converter at OFF-mode [39]

State equations of this mode can be expressed as,

$$l_1 \frac{\partial I_{l_1}}{\partial T} - V_{c_1} = 0 \tag{18}$$

$$l_2 \frac{\partial I_{l_2}}{\partial T} + V_{c_1} - V_{c_2} = 0 \tag{19}$$

$$c_1 \frac{\partial V_{c_1}}{\partial T} + I_{l_1} - I_{l_2} = 0 \tag{20}$$

$$c_2 \frac{\partial V_{c_2}}{\partial T} - I_{l_2} + \frac{1}{r_0} V_{c_2} = 0 \tag{21}$$

State space matrix model of ultra-lift luo converter in ON condition as follows,

$$\begin{bmatrix} I_{l_1} \\ I_{l_2} \\ I_{c_1} \\ I_{c_2} \end{bmatrix} = \begin{bmatrix} 0 & 0 & \frac{1}{l_1} & 0 \\ 0 & 0 & \frac{-1}{l_2} & \frac{1}{l_2} \\ \frac{-1}{c_1} & \frac{1}{c_1} & 0 & 0 \\ 0 & \frac{1}{c_2} & 0 & \frac{-1}{c_{2r_0}} \end{bmatrix} \begin{bmatrix} I_{l_1} \\ I_{l_2} \\ I_{c_1} \\ I_{c_2} \end{bmatrix} + \begin{bmatrix} 0 \\ 0 \\ 0 \\ 0 \end{bmatrix} V_{IN} \tag{22}$$

The state-space average model of ultra-lift luo converter is calculated using the combined form of equations (17) and (22) [39],

$$\dot{Z} = a_1 Z + b_1 V_{IN}, \tag{23}$$

When switch is ON (During $D \times t_s$)

$$\dot{Z} = a_2 Z + b_2 V_{IN}, \tag{24}$$

When switch is OFF (During (1- D) ×)

$$_{ts}\dot{Z} = [a_1 \times D + a_2 \times (1-D)] Z + [b_1 \times D + b_2 \times (1-D) V_{IN}] \tag{25}$$

$$\begin{bmatrix} I_{l_1} \\ I_{l_2} \\ I_{c_1} \\ I_{c_2} \end{bmatrix} = \begin{bmatrix} 0 & 0 & \frac{1(1-D)}{l_1} & 0 \\ 0 & 0 & \frac{-1}{l_2} & \frac{(1-D)}{l_2} \\ \frac{(D-1)}{c_1} & \frac{(1-2D)}{c_1} & 0 & 0 \\ 0 & \frac{(1-D)}{c_2} & 0 & \frac{-1}{c_2 r_0} \end{bmatrix} \begin{bmatrix} I_{l_1} \\ I_{l_2} \\ I_{c_1} \\ I_{c_2} \end{bmatrix} + \begin{bmatrix} 0 \\ 0 \\ 0 \\ 0 \end{bmatrix} V_{IN} \quad (26)$$

$$Y = \begin{bmatrix} V_0 \\ I_I \end{bmatrix} = \begin{bmatrix} 0 & 0 & 0 & 1 \\ D & D & 0 & 0 \end{bmatrix} \begin{bmatrix} I_{l_1} \\ I_{l_2} \\ I_{c_1} \\ I_{c_2} \end{bmatrix} \quad (27)$$

where,

Z Represent the vector with state variables, t_s represents the switching time along with D represent that duty cycle of converter switch.

3.3. Modelling of Cockcroft-Walton Multiplier

The Cockcroft-Walton is voltage multiplier used to convert AC or DC power as minimum voltage level to maximum DC voltage [40]. Unlike transformers, it neglects heavy core needs including most of the insulation / potting. It utilizes capacitors together with diodes in series circuit which helps to boost up the low voltages into high voltages. This multiplier has a simple structure and the cost is minimum than transformers. The figure 5 shows the equivalent circuit diagram of cockcroft-walton multiplier.
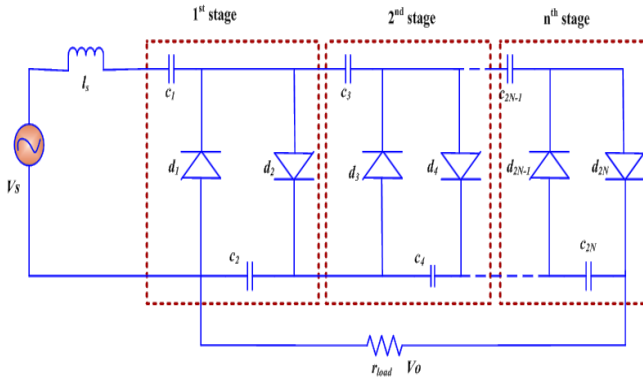

Figure 5. Equivalent circuit of Cockcroft-Walton multiplier [40]

Here, c_1, c_2, c_3,……,c_N represents the capacitors in N stages and d_1, d_2, d_3,……,d_N represents the diodes capacitors in N stages. In Cockcroft Walton multiplier, the peak-to-peak voltage in every stage is being double. The output voltage of Cockcroft Walton multiplier during no load condition may be articulated,

$$V_{out} = 2NV_{IN} \quad (28)$$

here, N is the number of stages, V_{IN} specifies input voltage of Cockcroft Walton multiplier, f is the switching frequency. The voltage deviation along voltage ripple is generated in its output voltage during the transmission of current. The voltage variation of Kth stage capacitor can be expressed as, , , n^{th} stage.

$$\varphi V_{c2K-1} = \varphi V_{c2K} = (N - K + 1) \frac{I_0}{fc} \quad (29)$$

The output voltage variation is similar to addition of an even capacitors voltage variation that may be denoted [40],

$$\varphi V_0 = \sum_{K=1}^{N} \varphi V_{2K} = \frac{N(N+1)}{2} \frac{I_0}{fc} \quad (30)$$

The voltage deviation of Kth stage even or odd capacitor is similar to addition of voltage variation as K^{th} stage.

$$\nabla V_{2K-1} = \sum_{I=1}^{K-1} \varphi V_{2I-1} = \frac{(N+K+1)(N-K)}{2} \frac{I_0}{fc} \quad (31)$$

$$\nabla V_{2K} = \sum_{I=1}^{K-1} \varphi V_{2I} = \frac{(N+K+1)(N-K)}{2} \frac{I_0}{fc} \quad (32)$$

The output voltage deviation is similar to addition of voltage deviation of even capacitors which can be expressed as,

$$\nabla V_o = \frac{(4N^3 + 3N^2 - N)(N-K)}{6} \frac{I_0}{fc} \quad (33)$$

The output voltage of cockcroft-walton multiplier with load may be expressed as [36],

$$V_o = 2NV_{IN} - \frac{(4N^3 + 3N^2 - N)}{6} \frac{I_0}{fc} \quad (34)$$

If the capacitors of all stages are equivalent, peak-to-peak high voltage pulse ripple of cockcroft-walton multiplier can be expressed as,

$$\varphi V_{PP} = \frac{N(N+1)p_0}{2fcV_o} \quad (35)$$

where, p_0 represent the output power, V_o represent the output voltage and c represents capacitance.

The ultra-lift luo converter and cockcroft-walton multiplier enhance the output voltage gain but which has some drawbacks like the delay between input and output, higher output voltage ripple and higher voltage deviation. To overcome these drawbacks and optimally increase the voltage gain for electric vehicle applications, a hybrid RFOA- DDAO technique is implemented with ultra-lift luo converter and cockroft-walton multiplier which is detail explained in the below section.

4. Proposed approach of red fox optimization algorithm (RFOA) and dynamic differential annealed optimization (DDAO) algorithm

The power flow among the load side and source side is clarified numerical designing in this part. The RES energy cache device is held in grid the power decided to provide. The linked system of MG is assured to the numerical designing, by energy source operation. The whole PF model of the system is believed among the order of load side and source side is situated on the power equivalent [40]. The generators and load necessities are used for the conclusion, the power correlative system is developed in grouping. Power correlative is detailed in eqn (26). To enhance that voltage gain without any voltage deviation and voltage ripples for driving the electric vehicle smoothly, a hybrid RFOA-DDAO technique is proposed in this work. The integration of RFOA and DDAO works with ultra-lift luo converter and Cockcroft Walton multiplier to make the result as best. The processing steps of red fox optimization algorithm and vehicle ad-hoc network optimization is explained in the below section.

4.1. Processing Steps of Red Fox Optimization Algorithm (RFOA)

The red fox population contains those who go into well-defined

territories and lead an itinerant life. All herds shear a particular territory in alpha pair hierarchy. While a youth fox increases up, it will come out from the herd and make its own herd and select the hunting area to start their hunting process. Else it stays with their parents and receives the hunting area based on their parent suggestions [41]. The red fox is a well-organized hunter of little animals. If it finds any animals in their surrounding place, it slowly moves towards those animals. At that time, if it finds another one prey, it suddenly stops their previous operation and thinks about to attack which prey. At that time, if it finds another one prey, it suddenly stops the previous operation and thinks about which prey should be attack. It selects the prey based on the distance. If the prey is far away from red fox, it rejects that prey and selects the closer one to attack. The calculation of distance of each individual in the population can be compute using the following expression,

$$D\left(\left(X^{I}\right)^{T},\left(X^{BEST}\right)^{T}\right)=\sqrt{\left(\left(X^{I}\right)^{T}-\left(X^{BEST}\right)^{T}\right)} \tag{36}$$

where,

X Represent the population; I represent the number of fox, X^{BEST} specifies best population and T represent the iteration number.

$$\left(X^{I}\right)^{T}=\left(X^{I}\right)^{T}+\beta\sin\left(\left(X^{BEST}\right)^{T}-\left(X^{I}\right)^{T}\right) \tag{37}$$

Each fox contains one fixed distance value for attacking the prey. If the distance of prey exceeds the fixed value, the fox waits and think about how to attack the prey, else it moves closer to the prey and starts to attack. For example,

$$\left.\begin{array}{ll} Move\ closer & if\ \ D<0.75 \\ Wait\ and\ think & if\ \ D>0.75 \end{array}\right\} \tag{38}$$

The step-by-step process of red fox optimization is shown below,

Step 1: Initialization
Initialize the input voltage, current and maximum iteration of the system. Also, initialize the population of red fox, corresponding searching area and preys using the following equation,

$$X=\left\{X_{0},X_{1},X_{2},.......X_{N}\right\} \tag{39}$$

$$A=\left\{A_{0},A_{1},A_{2},........A_{N}\right\} \tag{40}$$

$$P=\left\{P_{0},P_{1},P_{2},.......P_{N}\right\} \tag{41}$$

where, X specifies number of red fox, A specifies searching area and P is the number of prey.

Step 2: Random Generation
After the initialization procedure, randomly generate the input parameters using the following equation,

$$I=\begin{bmatrix} Z_{11} & Z_{12} & ... & Z_{1n} \\ Z_{21} & Z_{22} & ... & Z_{2n} \\ : & : & : & : \\ Z_{n1} & Z_{n2} & ... & Z_{nn} \end{bmatrix} \tag{42}$$

here, I represent the input parameters of the system.

Step 3: Fitness Function
Scale the fitness function for all iteration is expressed as,

$$OBJ=Max\sum_{I=1}^{n}VG_{I} \tag{43}$$

where, OBJ represent the objective function, Max represents the maximization, VG represent the voltage gain and I is the number of iterations. Once the objective function is accomplished, the process is optimal.

Step 4: Calculation
The distance of individuals in the population and motion of individuals towards the best hunting area can be computed using the following expression,

$$D\left(\left(X^{I}\right)^{T},\left(X^{BEST}\right)^{T}\right)=\sqrt{\left(\left(X^{I}\right)^{T}-\left(X^{BEST}\right)^{T}\right)} \tag{44}$$

$$\left(X^{I}\right)^{T}=\left(X^{I}\right)^{T}+\beta\sin\left(\left(X^{BEST}\right)^{T}-\left(X^{I}\right)^{T}\right) \tag{45}$$

Step5: Selection
Based on the distance of prey, the red fox selects the best one. If the distance is too large, the fox rejects that prey from the target list.

Step 6: Moving to a new position
After selecting the best prey, the red fox starts to slowly move towards the selected prey. It updates the position in step-by-step manner until closer to the prey. The new position updating can be expressed as,

$$\left\{ \begin{array}{c} X_{0}^{NEW}=AR.Cos(\psi_{1})+X_{0}^{ACTUAL} \\ X_{1}^{NEW}=AR.Sin(\psi_{1})+AR.Cos(\psi_{2})+X_{1}^{ACTUAL} \\ X_{2}^{NEW}=AR.Sin(\psi_{1})+AR.Sin(\psi_{2})+AR.Cos(\psi_{3})+X_{2}^{ACTUAL} \\ \vdots \\ X_{N-1}^{NEW}=AR.Sin(\psi_{1})+AR.Sin(\psi_{2})+\cdots++AR.Sin(\psi_{N-1})X_{N-1}^{ACTUAL} \end{array} \right. \tag{46}$$

Step 7: Attack Function
The attack can be modeled through a vector that starts from the current position of the red fox and ends at the location of the prey.

Step 8: Termination
If the process reaches an objective condition, it will be terminated otherwise it continues from step 3.

4.2. Processing Steps of Dynamic Differential Annealed Optimization (DDAO)

Basically, irons are melts into a liquid form at high temperature, then it comes into solid state on room temperature. Normally, multiple iron phases have grouped in the similar solid, and provides grouping of property with mechanic characteristics of steel. The dual-phase steel is created through the heating operation of iron at maximum temperature. Then the iron is rolled as thicker piece and cooled while rolling operation [42]. After that the different types of cooling is applied to the metal and finally the metal is cooled at room temperature. This operation creates steel using ferrite matrix microstructure consists of inflexible martensitic phase. The soft ferrite and hard marten site grouping provide dual phase steel through maximum strength using permittable rate of creation. Figure 6 shows the flowchart of RFOA-DDAO algorithm. The step-by-step process of DDAO algorithm is shown below,

Step 1: Initialization
Initially generate the input voltage and input current of the system, corresponding frequency limits and maximum iteration of the system. Also, initialize the mass of the steel and temperature range.
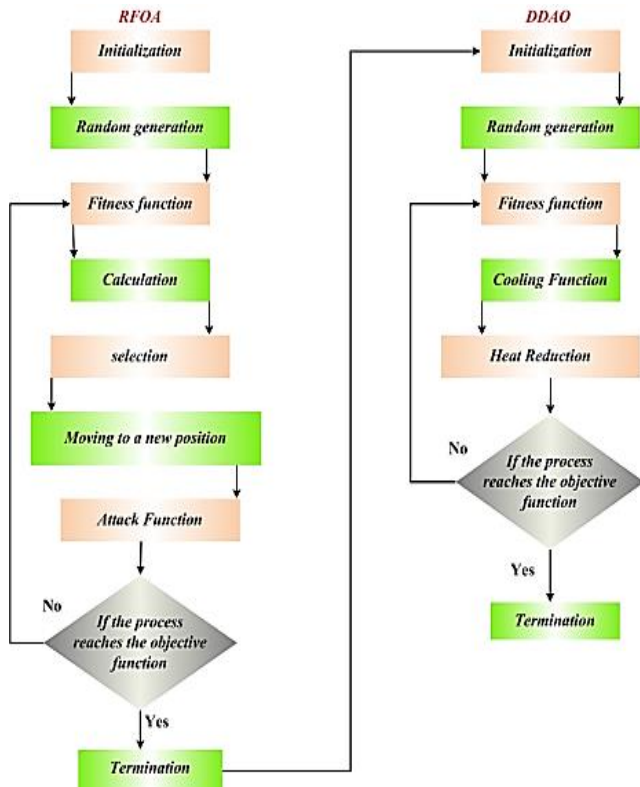
Figure 6. Flowchart of RFOA-DDAO algorithm

Step 2: Random Generation

After the process of initialization, the input parameters are generated randomly.

Step 3: Fitness Function

From the initialized values, the equation for the fitness function may be articulated,

$$F = MAX \sum_{I=1}^{N} VG_I \tag{47}$$

Once the objective function is accomplished, the process is optimal.

Step 4: Cooling Function

The following equation is utilized for evaluating the cooling function of the metal.

$$s^k = (sc_I - sc_J) + s_R \tag{48}$$

Where, the cooling solution with *I* and *J* indices are denoted as s^k

Step 5: Heat Reduction

The metals are becoming to forging state while the heat reduction function which can be expressed as,

$$F = \begin{cases} 1 \; if \; rem(iteration, 2) = 1 \\ random[0,1] \; if \; rem(iteration, 2) = 0 \end{cases} \tag{49}$$

Step 6: Termination

When the process reaches the objective condition, then it will be terminated otherwise it is continuing from step 3.

5. Results and discussion

This section describes that simulation result of proposed approach. To enhance the output voltage transfer gain for driving electric vehicles smoothly, RFOA-DDAO is implemented on this manuscript. The proposed strategy is executed through MATLAB/Simulink platform. The performance of proposed method is evaluated with comparison of existing methods like billiards inspired optimization algorithm (BOA) and giza pyramids construction (GPC). Figure 7 shows the analysis of converter input voltage. The input voltage of proposed converter is 40V from time period of 0sec to 5sec. Figure 8 shows the analysis of converter input current. Here, the converter input current is 6.35A at the time periods of 0.1sec, 0.2sec, 0.28sec, 0.36sec, 0.44sec, 0.52sec, 0.6sec, 0.68sec and 0.85sec. Figure 9 shows the analysis of voltage across D_2. The voltage across D_2 is 100V at starting stage then it reduced to 0 at 0.2sec. Further it increased to 100V and maintains constant until 0.2 to 0.2000. This same process is continuing from 0.2000sec to 0.2004sec. Figure 10 portrays that analysis of voltage across switch. Voltage across switch is 100V at starting stage then it reduced to 0 at 0.2sec. Further it increased to 100V and maintains constant until 0.2 to 0.2000. This same process is continuing from 0.2000sec to 0.2004sec. Figure 11 shows the analysis of current through l_1. The l_1 current is 6.4A at 0.1sec then it reduced to 5.6A at 0.12sec and maintains constant until 0.12sec to 0.17sec. After that it increased to 6.4A at 0.2sec then reduced to 5.6A at 0.21sec and also increased to 6.4A. This varying process is continuing until the time period of 0.9sec. Figure 12 shows the analysis of current through l_2. The l_2 current is 6A at 0sec then it reduced to 2.4A at 0.01sec. After that it increased to 2.5A at 0.02sec and the increasing process is continued until the time period of 0.1sec. Then it varies with constant manner until the time of 0.4sec. Figure 13 shows the analysis of voltage across c_1. The voltage across c_1 is -17.9V at 0.1sec then it increased to -17.878V at 0.11sec. After that it reduced to -17.905 at 0.13sec and this same varying process is continued until the time period of 0.7sec. Figure 14 shows the analysis of voltage across c_2. The voltage across c_2 is -17.95V at 0.4sec then it reduced to -17.91V at 0.402sec. After that it increased to -17.95 at 0.404sec and this same varying process is continued until the time period of 0.45sec. Figure 15 shows the analysis of converter output voltage. Here, the converter output voltage is 222V from the time period of 0sec to 5sec.
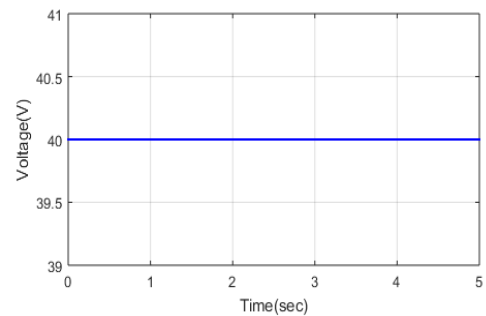

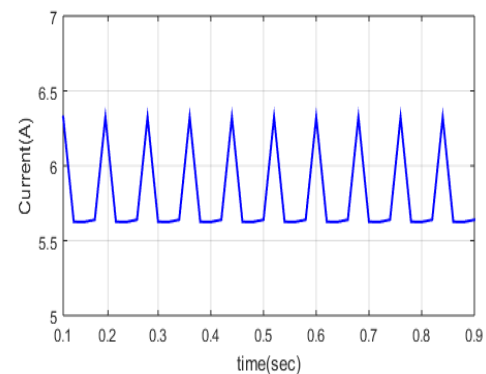**Figure 7.** Analysis of converter input voltage
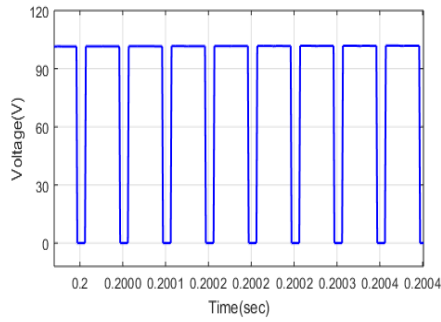

Figure 8. Analysis of converter input current
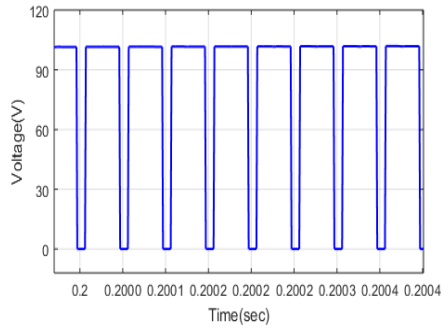
Figure 9. Analysis of voltage across D_2
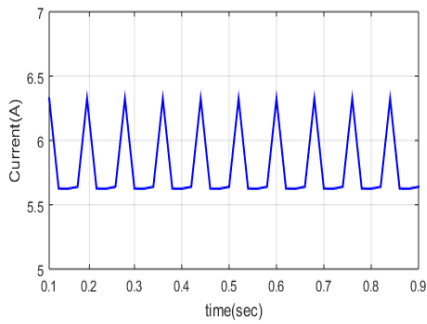

Figure 10. Analysis of voltage across switch

Figure 11. Analysis of current through l_1
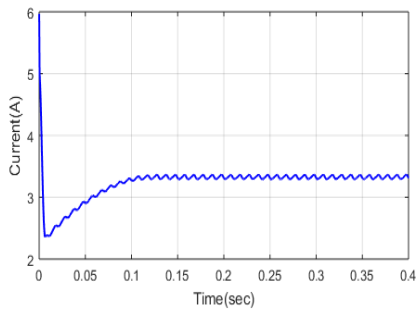

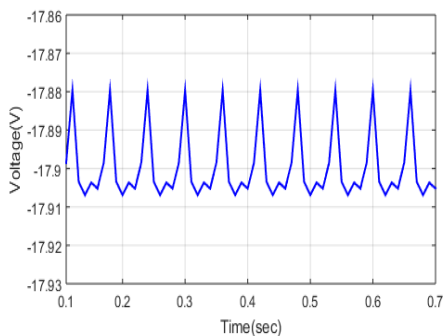**Figure 12.** Analysis of current through l_2

Figure 13. Analysis of voltage across c_1
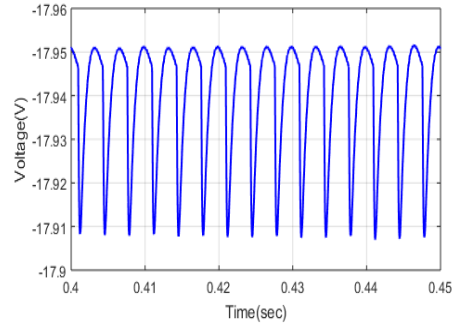

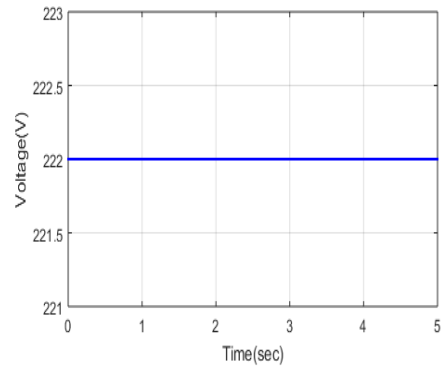**Figure 14.** Analysis of voltage across c_2

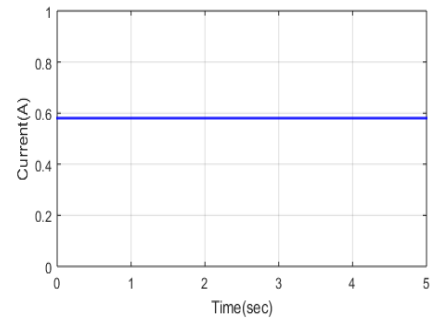**Figure 15.** Analysis of converter output voltage

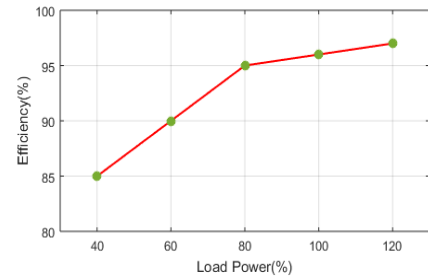**Figure 16.** Analysis of converter output current

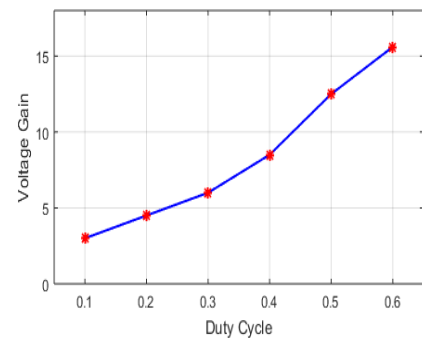**Figure 17.** Analysis of converter efficiency

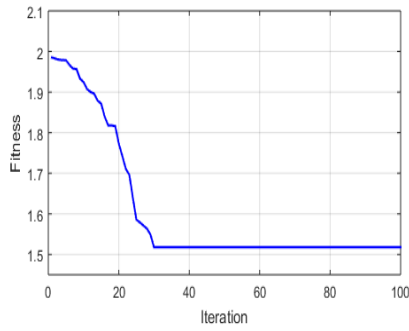**Figure 18.** Analysis of output voltage gain

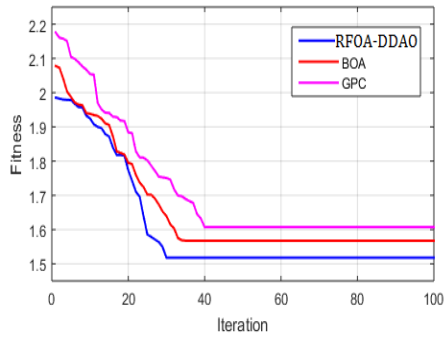**Figure 19.** Performance analysis of proposed method

Figure 20. Comparison performance of proposed using existing systems
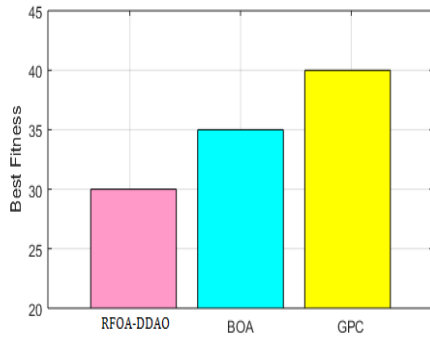

Figure 21. Comparison performance of proposed using existing systems
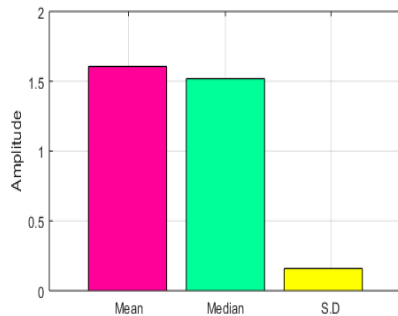

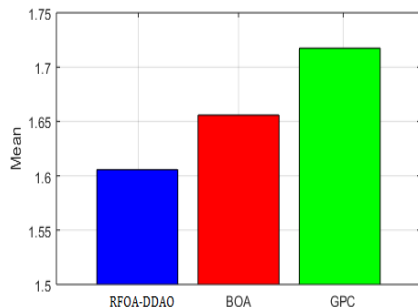**Figure 22.** Analysis of proposed mean, median and standard deviation (S.D)

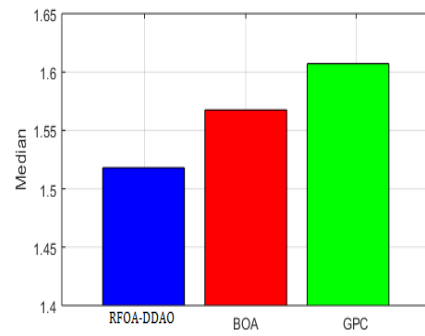**Figure 23.** Comparison of proposed mean using existing methods

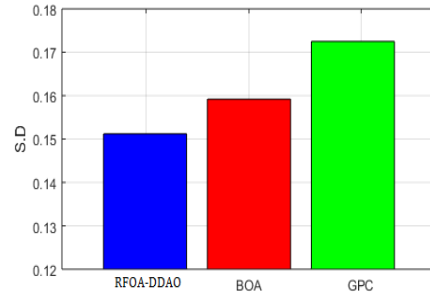**Figure 24.** Comparison of proposed median using existing methods

Figure 25. Comparison of proposed standard deviation with existing methods

Figure 16 shows the analysis of converter output current. Here, the converter output current is 0.6A from the time period of 0sec to 5sec. Figure 17 shows the analysis of converter efficiency. Here, the converter efficiency is 85% at the load power of 40%. Then it increased to 90% at load power 60%. When the load power is 80%, the efficiency reaches 95% and the efficiency is 96% at load power of 100%. Also, the efficiency is 97% at load power of 120%. Figure 18 shows the analysis of converter voltage gain. Here, the output voltage gain is 3.5 at the duty cycle of 0.1. Then it increased to 5 at duty cycle of 0.2. If duty cycle is 0.3, voltage gain reaches 6 and voltage gain is 12.5 at duty cycle 0.5. Also, voltage gain is 16 at duty cycle of 0.6. Figure 19 portrays that performance analysis of proposed method. Here, fitness of proposed method is 1.98 at first iteration and then the fitness is reduced to 1.52 at 30 iterations. Then the fitness maintains constant value of 1.52 until 100 iterations. Figure 20 depicts the comparison performance of RFOA-DDAO with existing methods. Here, fitness of RFOA-DDAO method is 1.98 at first iteration but the existing methods of BOA and GPC has the fitness of 2.09 and 2.19 at first iteration. Then the fitness of proposed method is reduced to 1.52 at 30 iterations but the fitness of existing methods like BOA and GPA is reduced to 1.58 at 31 iterations and 1.6 at 40 iterations. Then the fitness of proposed method maintains constant value of 1.52 from 30 to 100 iterations. Similarly, the existing methods maintain constant value until 100 iterations. Figure 21 displays the comparison performance of RFOA-DDAO with existing methods. Here, the RFOA-DDAO system consists of best fitness values to existing process. Figure 22 shows the analysis of proposed mean, median and standard deviation. Here, the proposed method has the mean values of 1.6 and median value of 1.5. The standard deviation of proposed method attains 0.2. Figure 23 depicts the comparison performance of proposed mean using existing systems. Here, the proposed mean is 1.6. The existing methods like BOA and GPC has the mean values of 1.65 and 1.72. The proposed system has best mean value to existing methods. Figure 24 shows the comparison performance of proposed median using existing systems. Here, the proposed median is 1.52. The existing methods like BOA and GPC has the median values of 1.57 and 1.61. The

proposed method has best median value than existing methods. Figure 25 represents the comparison performance of proposed standard deviation using existing methods. Here, the proposed standard deviation is 0.151. The existing methods like BOA and GPC has the median values of 0.16 and 0.172. The proposed method has best standard deviation value than existing methods.

Table 1: Parameters of ultra-liftluo converter

Parameters	Values
Input voltage	40V
Capacitors	$524\mu r$
Inductors	10mH
Switching frequency	50kHz
Output voltage	222V
Resistive load	$180\,\Omega$
Duty cycle	0.5

Table 2: Parameters of DDAO

Parameters	Values
Population size	3
Maximum temperature	50
Cooling rate	0.9996

Table 3: Parameters of RFOA

Parameters	Values
Population size	2
Number of iterations	20
Observation angle	270

Table 4: Analysis of proposed voltage gain with existing methods

Maximum voltage gain			% Voltage Enhancement in RFOA-DDAO
BOA	GPC	RFOA-DDAO	
11.11	14.34	16.01	5.25%

Table 5: Efficiency work out for proposed with existing techniques

Solution methods	Efficiency (%)
DE	79.265
ABC	82.237
PSO	87.1029
BOA	88.13
GPC	89.023
Proposed technique	95.4501

Table 1 describes the parameters in ultra-liftluo converter. Here, input voltage is 40V, capacitor value is 524524 μF, Inductor value is 10mH, switching frequency is 50 kHz, output voltage is 222V, resistive load is $180\,\Omega$ and duty cycle is 0.5. Table 2 describes the parameters of DDAO. The maximum population size is 3, maximum temperature is 50 and cooling rate is 0.9995. Table 3 describes the parameters of RFOA. The maximum population size is 2, number of iterations is 20 and the observation angle is 270. Table 4 describes the analysis of proposed voltage gain with existing methods. Here, the voltage gain of proposed method is 16.01%. But the voltage gain of existing methods like BOA and GPC is 11.11% and 14.34%. The proposed method provides maximum voltage gain than existing methods. Table 5 shows the efficiency work out for proposed with previous models.

6. Conclusion

This manuscript proposes a novel method to enhance the voltage transfer gain for derive an electric vehicle. The proposed hybrid technique with an ultra-liftluo converter and multiplier is suitable choice for running an electric vehicle smoothly. The proposed approach is providing a good and reliable result with lower count of iterations. The proposed method helps to make the calculations to easier and provides less complexity benefit. The proposed approach is executed in MATLAB/Simulink. The output is likened to existing BOA and GPC models. From comparison result, proposed method has greater voltage transfer gain, lower voltage ripple, lower voltage deviation and lower error which provide better performance than existing methods. Here, the discussing methods extend to other converters, viz boost, buck boost, other derivatives. In future, a higher step-up interleaved boost converter will simulate with various feedback control, viz FLC, GA, ANN for the enhancement of power quality or to get higher efficiency tuning, also verify the stable output voltage with least ripple and support various appliances with various voltage ratings.

References

[1] V. Kanamarlapudi, B. Wang, N. Kandasamy and P. So, "A New ZVS Full-Bridge DC–DC Converter for Battery Charging With Reduced Losses Over Full-Load Range,"IEEE Transactions on Industry Applications,vol.54, no.1 pp.571-579,2018.

[2] P. Tomar, M. Srivastava and A. Verma, "An Improved Current-Fed Bidirectional DC–DC Converter for Reconfigurable Split Battery in EVs,"IEEE Transactions on Industry Applications, vol.56, no.6, pp.6957-6967, 2020.

[3] L. Zhai, G. Hu, M. Lv, T. Zhang and R. Hou, "Comparison of Two Design Methods of EMI Filter for High Voltage Power Supply in DC-DC Converter of Electric Vehicle,"IEEE Access, vol8, pp. 66564-66577,2020.

[4] S. Lim, H. Lee, H. Cha and S. Park, "Multi-Level DC/DC Converter for E-Mobility Charging Stations,"IEEE Access, vol.8 pp.48774-48783, 2020.

[5] V. Kanamarlapudi, B. Wang, P. So and Z. Wang, "Analysis, Design, and Implementation of an APWM ZVZCS Full-Bridge DC–DC Converter for Battery Charging in Electric Vehicles,"IEEE Transactions on Power Electronics, vol.32, no.8, pp.6145-6160,2017.

[6] S. Assadi, H. Matsumoto, M. Moshirvaziri, M. Nasr, M. Zaman and O. Trescases, "Active Saturation Mitigation in High-Density Dual-Active-Bridge DC–DC Converter for On-Board EV Charger Applications,"IEEE Transactions on Power Electronics, vol.35, no.4,pp.4376-4387,2020.

[7] S. Kim, H. Cha and H. Kim, "High-Efficiency Voltage Balancer Having DC–DC Converter Function for EV Charging Station,"IEEE Journal of Emerging and Selected Topics in Power Electronics, vol.9, no.1,pp.812-821, 2021.

[8] N. Dao, D. Lee and Q. Phan, "High-Efficiency SiC-Based Isolated Three-Port DC/DC Converters for Hybrid Charging Stations,"IEEE Transactions on Power Electronics, vol.35, no.10, pp.10455-10465,2020.

[9] H. Moradisizkoohi, N. Elsayad and O. Mohammed, "A Voltage-Quadrupler Interleaved Bidirectional DC–DC Converter With Intrinsic Equal Current Sharing Characteristic for Electric Vehicles,"IEEE Transactions on Industrial Electronics, vol.68, no.2,pp.1803-1813,2021.

[10] R. Emamalipour and J. Lam, "A Hybrid String-Inverter/Rectifier Soft-Switched Bidirectional DC/DC Converter,"IEEE Transactions on Power Electronics, vol.35 pp.88200-8214,2020

[11] X. Ding, Y. Liu, D. Zhao and W. Wu, "Generalized Cockcroft-Walton Multiplier Voltage Z-Source Inverters," IEEE Transactions on Power Electronics, vol.35, no.7, pp.7175-7190, 2020.

[12] T.S. Maheshwari, P. Elangovan, S. Deepa. "Solar Energy Basedelectric Vehicle Using Super-Lift Converter with Battery." International Journal of Pure and Applied Mathematics, vo1.118, no.1, pp.443-450, 2018.

[13] Deepa Somasundaram, Samuel Babu, "A Closed Loop Control of Quadratic Boost Converter Using PID-controller" IJE TRANSACTIONS B: Applications Vol. 27, No. 11, pp.1653-1662, 2014.

[14] S. Mao, J. Popovic and J. Ferreira, "Diode Reverse Recovery Process and Reduction of a Half-Wave Series Cockcroft–Walton Voltage Multiplier for High-Frequency High-Voltage Generator Applications,"IEEE Transactions on Power Electronics, vol.34, no.2, pp.1492-1499,2019.

[15] A. Rajaei, R. Khazan, M. Mahmoudian, M. Mardaneh and M. Gitizadeh, "A Dual Inductor High Step-Up DC/DC Converter Based on the Cockcroft–Walton Multiplier,"IEEE Transactions on Power Electronics, vol.33, no.11,pp.9699-9709,2018.

[16] S. Park, J. Yang and J. Rivas-Davila, "A Hybrid Cockcroft–Walton/Dickson Multiplier for High Voltage Generation,"IEEE Transactions on Power Electronics, vol.35, no.3pp.2714-2723,2020.

[17] M. Quraan, A. Zahran, A. Herzallah and A. Ahmad, "Design and Model of Series-Connected High-Voltage DC Multipliers,"IEEE Transactions on Power Electronics, vol.35, no.7,pp.7160-7174,2020.

[18] A. Alzahrani, M. Ferdowsi and P. Shamsi, "A Family of Scalable Non-Isolated Interleaved DC-DC Boost Converters With Voltage Multiplier Cells,"IEEE Access, vol.7, pp.11707-11721,2019.

[19] S. Mythili, K. Thiyagarajah, P. Rajesh and Shajin FH. Ideal position and size selection of unified power flow controllers (UPFCs) to upgrade the dynamic stability of systems: an antlion optimiser and invasive weed optimisation algorithm. HKIE Trans, 27(1)(2020)25-37.

[20] P. Rajesh, F. A. Shajin. "Multi-Objective Hybrid Algorithm for Planning Electrical Distribution System," European Journal of Electrical Engineering, vol.22, no.1, pp.224-509, 2020.

[21] FH. Shajin, and P. Rajesh. "Trusted secure geographic routing protocol: outsider attack detection in mobile ad hoc networks by adopting trusted secure geographic routing protocol." International Journal of Pervasive Computing and Communications. 2020.

[22] MK., Thota, FH. Shajin and P. Rajesh. "Survey on software defect prediction techniques." International Journal of Applied Science and Engineering. Vol.17, no.4, pp.331-44, 2020.

[23] P. Upadhyay and R. Kumar, "A high gain cascaded boost converter with reduced voltage stress for PV application," Solar Energy, vol.183, pp.829-841, 2019.

[24] X. Dai, J. Jiang and J. Wu, "Charging Area Determining and Power Enhancement Method for Multiexcitation Unit Configuration of Wirelessly Dynamic Charging EV System," IEEE Transactions on Industrial Electronics, vol.66, no.5, pp.4086-4096, 2019.

[25] L. Lyu, X. Yang, Y. Xiang, J. Liu, S. Jawad and R. Deng, Exploring high-penetration electric vehicles impact on urban power grid based on voltage stability analysis, Energy, vol.198 pp.117301, 2020

[26] M. Bauer, J. Wiesmeier and J. Lygeros, "A comparison of system architectures for high-voltage electric vehicle batteries in stationary applications,"Journal of Energy Storage, vol.19, pp.15-27, 2018.;

[27] M. Kohli, and S. Arora, "Chaotic grey wolf optimization algorithm for constrained optimization problems." Journal of computational design and engineering, vol.5, no.4, pp.458-472, 2018

[28] F. K. Onay, and S. B. Aydemir, Chaotic hunger games search optimization algorithm for global optimization and engineering problems. Mathematics and Computers in Simulation, vol.192, pp.514-536, 2022.

[29] B. Alatas, Chaotic bee colony algorithms for global numerical optimization. Expert systems with applications, vol.37, no. 8, pp.5682-5687, 2010.

[30] B. Lee, J. Kim, S. Kim and J. Lee, "An Isolated/Bidirectional PWM Resonant Converter for V2G(H) EV On-Board Charger,"IEEETransactions on Vehicular Technology, vol.66, no.9, pp.7741-7750, 2017.

[31] Y. Zhang, H. Liu, J. Li, M. Sumner and C. Xia, "DC–DC Boost Converter With a Wide Input Range and High Voltage Gain for Fuel Cell Vehicles," IEEE Transactions on Power Electronics, vol.34, no.5, pp.4100-4111,2019

[32] Y. Zhang, C. Fu, M. Sumner and P. Wang, "A Wide Input-Voltage Range Quasi-Z-Source Boost DC–DC Converter With High-Voltage Gain for Fuel Cell Vehicles", IEEE Transactions on Industrial Electronics, vol.65, no.6, pp.5201-5212,2018.

[33] Y. Zhang, Q. Liu, Y. Gao, J. Li and M. Sumner, "Hybrid Switched-Capacitor/Switched-Quasi-Z-Source Bidirectional DC–DC Converter with a Wide Voltage Gain Range for Hybrid Energy Sources EVs," IEEE Transactions on Industrial Electronics, vol.66, no.4, pp.2680-2690,2019.

[34] J. Leyva-Ramos, R. Mota-Varona, M. Ortiz-Lopez, L. Diaz-Saldierna and D. Langarica-Cordoba, "Control Strategy of a Quadratic Boost Converter With Voltage Multiplier Cell for High-Voltage Gain," IEEE Journal of Emerging and Selected Topics in Power Electronics, vol.5, no.4, pp.1761-1770,2017.

[35] C. Lai, Y. Cheng, M. Hsieh and Y. Lin, "Development of a Bidirectional DC/DC Converter with Dual-Battery Energy Storage for Hybrid Electric Vehicle System," IEEE Transactions on Vehicular Technology, vol.67, no.2 pp.1036-1052,2018.

[36] Y. Zhang, Q. Liu, J. Li and M. Sumner, "A Common Ground Switched-Quasi-Z -Source Bidirectional DC–DC Converter With Wide-Voltage-Gain Range for EVs With Hybrid Energy Sources,"IEEE Transactions on Industrial Electronics, vol.65, no.6, pp.5188-5200,2018.

[37] Y. Zhang, Y. Gao, L. Zhou and M. Sumner, "A Switched-Capacitor Bidirectional DC–DC Converter With Wide Voltage Gain Range for Electric Vehicles With Hybrid Energy Sources,"IEEE Transactions on Power Electronics, vol.33 no.11, pp. 9459-9469,2018.

[38] D. Thomas, O. Deblecker and C. Ioakimidis, "Optimal operation of an energy management system for a grid-connected smart building considering photovoltaics' uncertainty and stochastic electric vehicles' driving schedule,"Applied Energy, vol.210, pp.1188-1206,2018.

[39] A. Sharifian, S. FathiSasansara, M. Ghadi, S. Ghavidel, L. Li and J. Zhang, "Dynamic performance improvement of an ultra-lift Luo DC–DC converter by using a type-2 fuzzy neural controller, "Computers& Electrical Engineering, vol.69, pp.171-182, 2018.

[40] S. Mao, J. Popovic and J. Ferreira, "Diode Reverse Recovery Process and Reduction of a Half-Wave Series Cockcroft–Walton Voltage Multiplier for High-Frequency High-Voltage Generator Applications,"IEEE Transactions on Power Electronics, vol.34, no.2, pp.1492-1499,2019.

[41] D. Połap and M. Woźniak, Red fox optimization algorithm, Expert Systems with Applications, vol. 166, pp.114107, 2021.

[42] H. Ghafil and K. Jármai, "Dynamic differential annealed optimization: New metaheuristic optimization algorithm for engineering applications," Applied Soft Computing, vol.93, pp.106392,2020.